
Unsupervised Semantic Attribute Discovery and Control in Generative Models

William Paul*, I-Jeng Wang*, Fady Alajaji⁺, Philippe Burlina*

*The Johns Hopkins University Applied Physics Laboratory, Laurel, MD 20723

⁺Department of Mathematics and Statistics Kingston, ON K7L 3N6, Canada

william.paul@jhuapl.edu, i-jeng.wang@jhuapl.edu
fa@queensu.ca, philippe.burlina@jhuapl.edu

Abstract

This work focuses on the ability to control – via latent space factors – semantic image attributes in generative models, and the faculty to discover mappings from factors to attributes in an unsupervised fashion. The discovery of controllable semantic attributes is of special importance, as it would facilitate higher level tasks such as unsupervised representation learning to improve anomaly detection, or the controlled generation of novel data for domain shift and imbalanced datasets.

The ability to control semantic attributes is related to the disentanglement of latent factors, which dictates that latent factors be ‘uncorrelated’ in their effects. Unfortunately, despite past progress, the connection between control and disentanglement remains, at best, confused and entangled, requiring clarifications we hope to provide in this work. To this end, we study the design of algorithms for image generation that allow unsupervised discovery and control of semantic attributes. We make several contributions: a) We bring order to the concepts of control and disentanglement, by providing an analytical derivation that connects mutual information maximization – which promotes attribute control – to total correlation minimization – which relates to disentanglement. b) We propose hybrid generative model architectures that use mutual information maximization with multi-scale style transfer. c) We introduce a novel metric to characterize the performance of semantic attributes control. We report experiments that appear to demonstrate, quantitatively and qualitatively, the ability of the proposed model to perform satisfactory control while still preserving competitive visual quality. We compare to other state of the art methods (e.g., Fréchet inception distance (FID) = 9.90 on CelebA and 4.52 on EyePACS).

1 Introduction

The transformative contribution of deep learning (DL) to AI, principally in discriminative models for supervised learning, has mostly hinged on the availability of large training datasets. Open problems still remain in DL, especially in unsupervised learning, inference on out-of-training-distribution test samples, domain shift, open set learning, and also in discriminative tasks where data is not easily obtained or when manual labeling is impractical or prohibitively onerous. Generative models – with their ability to generate new data and efficient representations of data – may assist in addressing some of these challenges.

Considering these challenges, the ability to generate images at will that allow the discovery and control of individual semantic images attributes, via latent space factors, is of paramount importance. Generative methods – broadly speaking – learn to sample from the underlying training data distribution so as to generate new samples that are distinct from, but visually or statistically indistinguishable

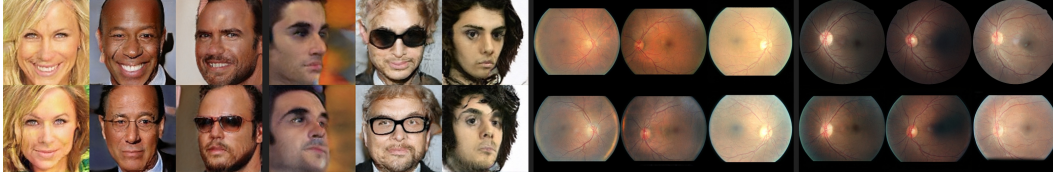


Figure 1: Demonstrated control of our proposed algorithm InfoStyleGAN on the two used datasets: faces (CelebA) and medical/retinal (EyePacs). The rows denote a change in a single variable, while the columns denote different samplings of the rest of the latent factors. For faces, the first group (from left to right) demonstrates control over smiling (columns 1-3) and background color; the second group (columns 4-6) demonstrates orientation of the head. For retinal images, the third group (columns 7-9) demonstrates control over melanin content, while the last group (columns 10-12) shows control of the field of view and the amount of glare on the retina.

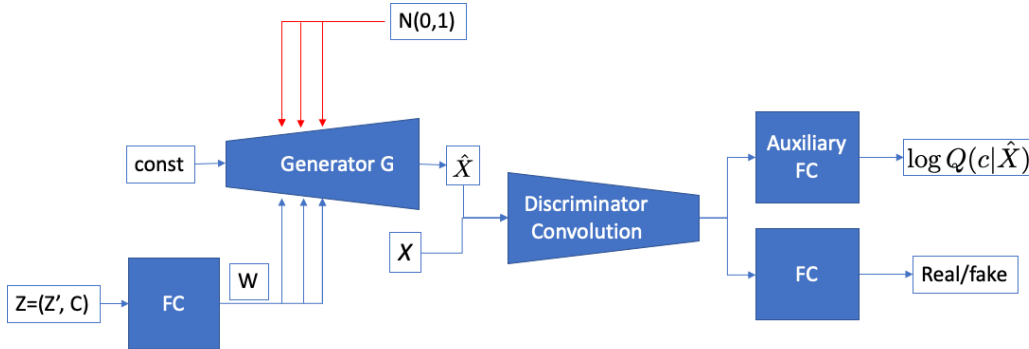


Figure 2: Our proposed multi-scale generator and discriminator architecture: the latent vector Z is split into a semantic vector C and noise vector Z' . A sample (z', c) is then fed into a mapping network to produce an intermediate latent vector W which in turn is fed into the generator. Mutual information maximizing loss is used between the latent and output generated images, combined with a conditional loss and a traditional GAN adversarial loss.

from, the underlying training data. A simple taxonomy of generative models includes: generative adversarial networks (GANs) in [5] and [17], autoencoders/variational autoencoders (VAEs) in [10], and, used to a lesser extent, compared to the aforementioned ones, generative autoregressive models in [15], invertible flow based latent vector models in [11], or hybrids of the above models as in [6].

Prior and recent research in generative models inspiring, and limitations motivating, our work includes the following areas of research.

Best of Breed GAN Approaches

Only recently have GANs been able to generate images at relatively high resolutions (greater than 256×256 pixels). Examples of methods that achieve such results include ProGAN [7], BigGAN [1], and COCO-GAN [12]. For example, BigGAN relied on SAGAN [18] as a baseline (self attention GANs). The study noted the strong effect of large batch sizes on performance (multiplying batch size by a factor of 8 leads to over 40% increase in inception score over other state of the art algorithms). The study noted also that larger networks had a comparable positive effect, and so did the usage of the *truncation* trick (i.e., for the generator, sampling from a standard normal distribution in training while sampling instead from a truncated normal distribution in inference, where samples that are above a certain threshold are re-sampled). Truncating with a lower threshold allowed control of the trade-off between higher fidelity and lower diversity.

Unfortunately, while many best of breed generative approaches make progress in terms of visual quality and high resolutions, these methods cannot directly be used for semantic attribute control, which motivated our work.

Style Transfer

Karras et al. recently developed StyleGAN which used a multi-scale design [8]. StyleGAN has been very successful at addressing the generation of high dimensional images (1024×1024), and are an extension of ProGAN that was based on progressively growing the encoder and decoder/discriminator in GAN networks. Some of the specific novel features in [8] consisted of injecting noise at every scale resolution of the decoder, and using a fully connected (FC) network that mapped a latent vector Z into a 512-length intermediate latent vector W that controls the generation of images (a so called 'style' vector). This style vector W is used to control some attributes of the image (at the low scale coarse attributes like skin tone and at the higher scale fine attributes like hair).

An updated version of StyleGAN [9], StyleGAN2, introduced architectural improvements, along with an improved projection method for mapping images to latent spaces.

While both methods allow for attribute style mixing, there is no way to specifically control image attributes without an existing image that exhibit desired attributes. This existing image could also have undesirable attributes that are also transferred. In contrast, the approach we take strives for the isolation of desirable from undesirable attribute.

Other notable recent studies in DL that borrowed from Information Theoretic concepts and inspired our study include:

Information Theoretic Approaches

In [3], InfoGAN made use for the first time of the principle of maximizing the mutual information $\mathbb{I}(C; \hat{X})$ between semantic vector C and the generated image \hat{X} , where C is a semantic component of the latent vector representation $Z = (Z', C)$ with Z' being a noise vector. This process was set up to achieve disentanglement in latent factors. Experiments exemplified various degrees of connection between such factors and semantic attributes. However, as our study should demonstrate, while the mutual information principle promotes the control of attributes in images, true disentanglement is not achieved via this maximization of mutual information. Indeed, the results in [3] suggested various degree of success and consistency between the ability of the network to actually control and disentangle.

Instead, we believe the concept of disentanglement was appropriately defined in [2], as the process of finding latent factors that satisfy minimum total correlation. Total correlation is defined as the divergence between the joint distribution and the product of the marginals. In this study, we adopt this definition and demonstrate how it relates to the concept of control and maximization of mutual information. Despite this contribution, the concepts of control and disentanglement remained confused with each other.

Contribution

In sum, looking at past contributions, despite great progress made in the areas of disentanglement and control, work remains to bring order in those concepts, which we pursue in this paper. Therefore, the contributions of this work are as follows:

- a) We bring order to the concepts of control and disentanglement, by providing an analytical derivation that connects mutual information maximization – which promotes attribute control – to total correlation minimization – which relates to disentanglement.
- b) We study hybrid generative model architectures that use mutual information maximization with multiscale style transfer, called InfoStyleGAN.
- c) We introduce a novel metric and provide experiments that appear to demonstrate quantitatively and qualitatively the ability of the proposed models with regard to performing satisfactory semantic attribute control, while preserving competitive FIDs, when compared to other state of the art methods – some which may not even allow for attribute control – when using models of similar size (e.g., FID = 9.90 on CelebA and 4.52 on EyePACS).

2 Methods

We describe the approach in the next sections including details on the architecture, loss functions and training methods.

2.1 Architecture

The model’s components used here are depicted in Figure 2. The architecture utilizes multiscale GAN subcomponents similar to [8] (generator and adversarial discriminator), as follows: a) a generator $\hat{X} = \mathcal{G}(Z)$ including a mapping from a latent space vector to a style vector via a FC network, and a multiscale generator (decoder) that starts with a 4×4 image and builds up to a 1024×1024 image, and takes both noise input, and input from the style vector (after adaptive instance normalization), at every scale, and generates an output image \hat{X} . The model’s architecture then includes additional components described next to achieve attribute control.

Since we seek image attribute control and latent space factor disentanglement, we split the latent vector $Z = (Z', C)$ into a standard Gaussian noise vector Z' and a latent vector component C (henceforth called the vector of latent factors) with distribution $p(C)$, where C and Z' are independent of each other. For disentanglement, the concept of total decorrelation between the different *latent factors* of C is used. Furthermore for discovery and control of *semantic image attributes*, the concept of *maximization of mutual information* with the latent factors is invoked. The latter concept is explicitly used in our approach. We will later demonstrate analytically that the former concept of decorrelation results – under certain conditions – from the later mutual information maximization principle.

Control via maximization of the mutual information (MI): the idea here is to maximize the mutual information $I(C; \mathcal{G}(Z', C))$ between the semantic vector C and the observation $\hat{X} = \mathcal{G}(Z', C)$ as a means of coupling the vector C to the different variations of the images X in the dataset. Since computing mutual information (MI) is complicated by the fact it entails knowing the posterior $p(C|\hat{X})$, one can instead, as in [3], employ an auxiliary distribution $\mathcal{Q}(C|\hat{X})$ that approximates this posterior and that can be selected to maximize the mutual information.

Disentanglement via minimization of total correlation: Although InfoGAN [3] introduced an auxiliary loss to maximize the mutual information between $C = (C_1, C_2, \dots, C_L)$, where each C_i can be governed by a different distribution, and $\hat{X} = \mathcal{G}(Z', C)$, where Z' is an additional noise vector, there is no explicit objective for controlling a diverse set of image attributes. For example, even with the independence implementation on the prior $p(C) = \prod_i p(C_i)$, all semantically relevant variables could only seemingly affect the skin in faces, with different variables focusing on skin tone, skin texture, glare on the skin, etc. In effect, despite being sampled as independent, the effect between individual variables on the image are highly correlated. Consequently, a desirable end goal for disentanglement is that knowledge of one latent factor from the image does not affect the knowledge of other latent factors; i.e., having $p(C|\hat{X} = \hat{x}) = \prod_i p(C_i|\hat{X} = \hat{x})$ or conditional independence of the true posterior of the latent factors given a realization $\hat{X} = \hat{x}$ of the generated image. This is equivalent to having $\mathbb{T}\mathbb{C}(C|\hat{X} = \hat{x}) = 0$, where $\mathbb{T}\mathbb{C}(\cdot|\hat{X} = \hat{x})$ is the total correlation [2] given $\hat{X} = \hat{x}$, defined as the Kullback-Leibler (KL) divergence, denoted by $D_{KL}(\cdot||\cdot)$, between the conditional joint distribution given $\hat{X} = \hat{x}$ and the product of the conditional marginal distributions given $\hat{X} = \hat{x}$, i.e.,

$$\mathbb{T}\mathbb{C}(C|\hat{X} = \hat{x}) = D_{KL} \left(p(C|\hat{X} = \hat{x}) \parallel \prod_i p(C_i|\hat{X} = \hat{x}) \right). \quad (1)$$

We will argue that the previous two concepts are connected to each other as shown later in Lemma 3.1. Indeed, under certain assumptions, maximization of mutual information constrains down the total correlation. Therefore only the mutual information constraint will be considered henceforth.

2.2 Loss Function

The loss function is comprised of two parts: the adversarial loss $V(\mathcal{D}, \mathcal{G})$ for the generator \mathcal{G} and discriminator \mathcal{D} as well as the lower bound $L_{\text{info}}(\mathcal{G}, \mathcal{Q})$ on the mutual information;

$$V(\mathcal{D}, \mathcal{G}) = \mathbb{E}_{C \sim p(C), \hat{X} \sim \mathcal{G}(Z', C)} (\log(1 - \mathcal{D}(\hat{X}))) + \mathbb{E}_X (\log(\mathcal{D}(X))) \quad (2)$$

$$L_{\text{info}}(\mathcal{G}, \mathcal{Q}) = \mathbb{E}_{C \sim p(C), \hat{X} \sim \mathcal{G}(Z', C)} (\log(\mathcal{Q}(C|\hat{X})) - \log p(C)) \quad (3)$$

with $\mathbb{E}(\cdot)$ denoting the expectation operator and $0 \leq \mathcal{D}(\cdot) \leq 1$. Note that we abused the notation in $\hat{X} \sim \mathcal{G}(Z', C)$ to denote the conditional distribution $p(\hat{X}|C)$ given C (this conditional distribution

is intrinsically determined by the distribution of Z'). The optimization problem consists then of determining the triplet $(\mathcal{D}, \mathcal{G}, \mathcal{Q})$ that achieves:

$$\min_{\mathcal{G}, \mathcal{Q}} \max_{\mathcal{D}} V(\mathcal{D}, \mathcal{G}) - \beta L_{\text{info}}(\mathcal{G}, \mathcal{Q}) \quad (4)$$

where coefficient $\beta \geq 0$ is a hyper-parameter and \mathcal{Q} is the auxiliary network which computes the parameters of the distribution of C given \hat{X} used to evaluate $\mathcal{Q}(C|\hat{X})$.

Monte Carlo estimates of $V(\mathcal{D}, \mathcal{G})$ and $L_{\text{info}}(\mathcal{G}, \mathcal{Q})$, $\tilde{V}(\mathcal{D}, \mathcal{Q})$ and $\tilde{L}_{\text{info}}(\mathcal{G}, \mathcal{Q})$ respectively, are used for tractable optimization of the above. Using a batch size B , $\{z'(l), c'(l)\}_{l=1}^B$ is sampled from Z , as Z is explicitly defined, and then fed into the generator to produce the fake image $\hat{x}(l) = \mathcal{G}(z'(l), c'(l))$ B times, as well as the real images $x(l)$ being sampled B times. The estimates for the losses are thus:

$$\begin{aligned} \tilde{V}(\mathcal{D}, \mathcal{G}) &= \frac{1}{B} \sum_{l=1}^B (\log(1 - \mathcal{D}(\hat{x}(l))) + \log(\mathcal{D}(x(l))), \\ \tilde{L}_{\text{info}}(\mathcal{G}, \mathcal{Q}) &= \frac{1}{B} \sum_{l=1}^B (\log(\mathcal{Q}(c'(l)|\hat{x}(l))) - \log p(c'(l))). \end{aligned}$$

We henceforth refer to the family of algorithms the above model subsumes as MSI – for Multi-Scale Information theoretic. For notation, $\text{MSI}(S, \beta, d)$ is used, where S is a binary variable indicating whether styles such as from [8] are used, β denotes the coefficient used in Equation (4), and d is a binary variable to indicate if only discrete variables were used in C (if $d = 0$, then both continuous and discrete variables were used). In particular, $\text{MSI}(S = 0, \beta = 1, d = 0)$ results in InfoGAN, $\text{MSI}(S = 1, \beta = 0, d = 0)$ in StyleGAN, and $\text{MSI}(S = 1, \beta = 1, d = 0)$ in *InfoStyleGAN*.

3 Analysing Mutual Information Maximization and Decorrelation

We present a lemma that the choice of the mean field encoder, i.e., using $\mathcal{Q}(C|\hat{X}) = \prod_i \mathcal{Q}(C_i|\hat{X})$, for optimizing the mutual information (as used in [3]) contributes to forcing the total correlation to zero.

Lemma 3.1. Assume that each C_i is discrete for $i = 1, \dots, L$ (hence $\mathbb{I}(C; \hat{X})$ is bounded from above) and that $\mathcal{Q}(C|\hat{X}) = \prod_i \mathcal{Q}(C_i|\hat{X})$. When $L_{\text{info}} \rightarrow \mathbb{I}(C; \hat{X})$, then $\mathbb{TC}(C|\hat{X}) \rightarrow 0$ almost everywhere.

Proof. First, recall the derivation of the InfoGAN objective from [3]:

$$\begin{aligned} \mathbb{I}(C; \hat{X}) &= -\mathbb{H}(C|\hat{X}) + \mathbb{H}(C) \\ &= \mathbb{E}_{\hat{X}} [\mathbb{E}_{C' \sim p(C|\hat{X})} (\log p(C'|\hat{X}))] + \mathbb{H}(C) \end{aligned} \quad (5)$$

$$\begin{aligned} &= \mathbb{E}_{\hat{X}} [\underbrace{D_{KL}(p(C|\hat{X})\| \mathcal{Q}(C|\hat{X}))}_{\geq 0} + \mathbb{E}_{C' \sim p(C|\hat{X})} (\log \mathcal{Q}(C'|\hat{X}))] + \mathbb{H}(C) \\ &\geq \mathbb{E}_{\hat{X}} [\mathbb{E}_{C' \sim p(C|\hat{X})} (\log \mathcal{Q}(C'|\hat{X}))] + \mathbb{H}(C) \end{aligned} \quad (6)$$

$$\begin{aligned} &= \mathbb{E}_{C \sim p(C), \hat{X} \sim \mathcal{G}(Z', C)} (\log \mathcal{Q}(C|\hat{X})) + \mathbb{H}(C) \\ &= L_{\text{info}} \end{aligned}$$

where $\mathbb{H}(\cdot)$ and $\mathbb{H}(\cdot|\cdot)$ denote entropy and conditional entropy, respectively. Note that $\mathbb{H}(C) = \sum_i \mathbb{H}(C_i)$ as we assume the prior to the generative model factorizes independently.

Starting from (5), we can decompose the logarithmic term for each individual C_i to get:

$$\begin{aligned} \mathbb{I}(C; \hat{X}) &= \mathbb{E}_{\hat{X}} \left[\mathbb{E}_{C' \sim p(C|\hat{X})} \left(\log \frac{p(C'|\hat{X})}{\prod_i p(C'_i|\hat{X})} \right) \right] \\ &\quad + \sum_i \left(\mathbb{E}_{\hat{X}} [\mathbb{E}_{C'_i \sim p(C_i|\hat{X})} (\log p(C'_i|\hat{X}))] + \mathbb{H}(C_i) \right) \end{aligned} \quad (7)$$

$$= \mathbb{E}_{C \sim p(C), \hat{X} \sim \mathcal{G}(Z', C)} (\mathbb{TC}(C|\hat{X})) + \sum_i \mathbb{I}(C_i; \hat{X}). \quad (8)$$

Now, purely maximizing the mutual information with respect to all variables could also increase the total correlation of the posterior $p(C|\hat{X})$ of a fake image \hat{X} , implying that the factors given the image are more entangled, which is undesirable. Thus, we desire a low total correlation \mathbb{TC} and high mutual information \mathbb{I} between \hat{X} , the generated image, and each variable C_i individually, which we argue that the original InfoGAN objective implicitly satisfies for discrete (finite-valued) variables.

Indeed, we can lower bound each individual $\mathbb{I}(C_i; \hat{X})$ term in (8) via the same method as in (6): we have

$$\mathbb{H}(C) \geq \mathbb{I}(C; \hat{X}) \tag{9}$$

$$\geq \mathbb{I}(C; \hat{X}) - \mathbb{E}_{C \sim p(C), \hat{X} \sim \mathcal{G}(Z', C)}(\mathbb{TC}(C|\hat{X})) \tag{10}$$

$$= \sum_i \mathbb{I}(C_i; \hat{X}) \tag{11}$$

$$\geq \sum_i \left(\mathbb{E}_{\hat{X}} [\mathbb{E}_{C_i \sim p(C_i|\hat{X})}(\log \mathcal{Q}(C_i|\hat{X}))] + \mathbb{H}(C_i) \right) \tag{12}$$

$$= \mathbb{E}_{C \sim p(C), \hat{X} \sim \mathcal{G}(Z', C)}(\log \mathcal{Q}(C|\hat{X})) + \mathbb{H}(C) = L_{\text{info}} \tag{13}$$

where (11) holds by (8), (12) follows from (6) applied to each $\mathbb{I}(C_i; \hat{X})$ term. The equality before last is due to our assumption of a mean field encoder and the fact that $p(C) = \prod_i p(C_i)$.

Thus, when $L_{\text{info}} \rightarrow \mathbb{I}(C; \hat{X})$, the two inequalities in (10) and (12) become tight, in turn implying that $\mathcal{Q}(C|\hat{X}) \rightarrow p(C|\hat{X})$ and that $\mathbb{TC}(C|\hat{X}) \rightarrow 0$ almost everywhere in \hat{X} . \square

As explained earlier this lemma only applies to discrete random vectors. Nevertheless it provides useful insight regarding the connection between MI maximization and total correlation minimization.

4 Experiments, Additional Implementation Considerations and Performance Characterization

Many of the settings from the implementation of [8] are used here: mixing is turned off, as it was found that mixing the styles reduces disentanglement. Also having different semantic factors comprising the image may harm optimizing the lower information bound. For computational efficiency, we append \mathcal{Q} to \mathcal{D} as shown in Figure 2 above similar to [3]. We use a 512 dimension latent vector for (Z', C) . More implementation details follow.

We apply the method to two datasets: CelebA, to see the quantitative and qualitative improvement over state of the art systems for high resolution images, and EyePACS, to see how this method fares on a higher resolution medical image public dataset that includes wider variations in semantic features not present in faces such as retinal vasculature. We evaluate results qualitatively via visual inspection as well as quantitatively using FID.

4.1 CelebA

We use the aligned version of CelebA [13], with a 128×128 resolution and 202,599 images. Consistent with our method, we do not use the image labels with CelebA during training, as they comprise of individual binary image attributes that should be learned explicitly.

For the semantically relevant factors, we chose C to have: 1 categorical variable of dimension 3, 7 Bernoulli variables, and 10 uniform variables. The auxiliary network uses the same distributions for prediction, except that the uniform variables are treated as Gaussian (normal) with fixed unit variance.

For the implementation, mixing is turned off, and progressive growing starts at 8×8 resolution. The learning rate is 0.001 for resolutions below 128×128 , and becomes 0.003 at 128×128 . Gradient penalty on the real image loss for the discriminator is set at 10. The batch size is 1024 for resolution of 8×8 , 512 for resolutions of 16×16 and 32×32 , 256 for 64×64 , and 128 for resolution of 128×128 . The network is trained for 55 million images, or roughly 275 epochs. For CelebA, we also train $MSI(S = 1, \beta = 0, d = 0)$ as a baseline for visual quality, and $MSI(S = 0, \beta = 1, d = 0)$ as a baseline for controlling semantic features.

4.2 EyePACS

To see the effects of including the mutual information on higher resolution images on a medical domain with challenges other and more extensive than faces, we turn to the EyePACS dataset in [4], a diabetic retinopathy (DR) dataset of 53,576 retinal images with very high resolution that are downsampled to resolution 512×512 pixels. There are image labels associated with this describing the level of diabetic retinopathy (5 levels going from 0 = No DR, 1 = Mild, 2 = Moderate, 3 = Severe, 4 = Proliferative DR), which we use in the loss function with labels in Equation (2).

Most of the training details carry over from CelebA, except for the higher used resolution. Again, we turn mixing off, and train for 20 million images, or roughly 350 epochs. The batch sizes for 256×256 and 512×512 resolutions are 64 and 32 respectively.

4.3 Quantitative Assessment of Generative Quality and Diversity, and Faculty for Attribute Control

Although several metrics have emerged to characterize quality and diversity in generative models, we use FID as our primary measure of distance, which is computed as:

$$FID = \|\mu_r - \mu_g\|^2 + \text{Tr}(\Sigma_r + \Sigma_g - 2(\Sigma_r \Sigma_g)^{0.5}) \quad (14)$$

where $\|\cdot\|^2$ and $\text{Tr}(\cdot)$ denote the L_2 norm and the trace, respectively, and the assumption is made that $X_r \sim \mathcal{N}(\mu_r, \Sigma_r)$, i.e., a normal distribution (with mean-vector μ_r and covariance matrix Σ_r) for the activations from the Inception v3 pool layer for real examples, and likewise $X_g \sim \mathcal{N}(\mu_g, \Sigma_g)$ for generated examples.

FID is reported for each of the architectural variants of the MSI family of algorithms, and both datasets, as shown in Table 1. Additionally comparisons are shown in the last rows and taken from [14], where the training scheme is different; that study used a smaller architecture and a 64×64 resolution version of CelebA. All three models are on par with each other in terms of pure visual quality.

In order to characterize the ability of the algorithms to control individual image attributes of generated images, we also utilize two additional metrics, the mutual information gap (MIG) [2] as well as a metric we call the Attribute Control Metric (ACM). Both are detailed next.

Mutual Information Gap: As we have ground truth attribute labels for CelebA describing various semantic attributes $\{V_k\}_{k=1}^K$, where K is the number of ground truth attributes, we can use those directly in a supervised fashion to estimate the mutual information between each V_k and each C_i , $i = 1, \dots, L$, as described by the auxiliary network \mathcal{Q} . Consequently, we estimate the mutual information between V_k and C_i as

$$\mathbb{I}(V_k; C_i) = \mathbb{E}_{V_k, C'_i \sim \mathcal{Q}(C_i|V_k)} \left(\log \sum_{\tilde{x} \in X_{V_k}} \mathcal{Q}(C'_i|\tilde{x}) p(\tilde{x}|V_k) \right) + \mathbb{H}(C_i)$$

over k and i , where X_{v_k} is the set of images that correspond to having the label v_k . As the overall conditional probability $p(\tilde{x}|v_k)$ is unknown, we assume a uniform distribution over all \tilde{x} that have v_k as a label. The MIG is then

$$MIG = \frac{1}{K} \sum_{k=1}^K \frac{1}{\mathbb{H}(V_k)} \left(\mathbb{I}(V_k; C_{i(k)}) - \max_{i \neq i(k)} \mathbb{I}(V_k; C_i) \right) \quad (15)$$

where

$$i(k) = \text{argmax}_i \mathbb{I}(V_k; C_i) \quad (16)$$

is the index over the latent factors C_i that selects the C_i with the maximum mutual information with respect to the given ground truth attribute. Consequently, the MIG is the normalized difference between the maximum and second largest mutual information. For CelebA, the set of attributes $\{V_k\}$ consists of 40 attributes, including binary variables for smiling, attractiveness, etc.

There are two consequences of using this measure: (1) a larger value indicates that the information about a ground truth attribute is concentrated in a single latent factor which aligns with the goals

of disentanglement and (2) a small value does not necessarily indicate that our model does not successfully disentangle but that the semantic attributes it discovers may not align with any of the ground truth semantic attributes. Consequently, we also include the maximum mutual information to indicate if this is occurring.

From Table 2, we see that InfoStyleGAN for CelebA does improve upon disentanglement compared to InfoGAN.

Attribute Control Metric: As we do not have labels describing individual attributes for EyePACS, we manually choose out of C a variable c_i that appears to best control a discernible semantic image attribute. We sample N examples from Z , and evaluate each image as we vary c_i (here $N=100$). For our chosen c_i , we then estimate the percentage of examples where it did actually control the attribute consistently, as shown in Table 3.

Models	CelebA	EyePACS
MSI($S = 0, \beta = 1, d = 0$)	9.91 (± 0.06)	5.15 (± 0.03)
MSI($S = 1, \beta = 0, d = 0$)	9.08 (± 0.10)	4.11 (± 0.02)
MSI($S = 1, \beta = 1, d = 0$)	9.90 (± 0.07)	4.52 (± 0.03)
MSI($S = 1, \beta = 1, d = 1$)	14.3 (± 0.05)	9.59 (± 0.10)
WGAN GP*	30.0	†
BEGAN*	38.9	†
DRAGAN*	42.3	†
COCO-GAN*	4.2	†

Table 1: Quality of generated images: This table demonstrates that adding disentanglement properties does not negatively impact visual performance (FID). Best FID found during training for various architectures including our MSI (Multi-Scale Information theoretic) algorithm, with standard deviations taken over five estimates of the metric. MSI(S, β, d) denotes variations of our algorithm, where S indicates if styles are used, β is the coefficient on the information term, and d denotes if only discrete variables are used in C . FID is competitive even including the information loss term, showing that the additional term does not harm performance significantly. FIDs are also reported for CelebA for other competing state of the art (SOTA) generative models that are however non-disentangling algorithms as reported in [14], denoted by *. † indicates that no results are known, to the best of our knowledge, for those entries. The combination of visual inspection, which demonstrate disentanglement for our proposed full fledged algorithm, combined with the comparatively competitive FID (when compared to our ablated baselines and other SOTA algorithms), suggest the benefit of our proposed method.

Models	MIG	$\max_{k,i} \mathbb{I}(V_k; C_i)$
MSI($S = 0, \beta = 1, d = 0$)	2.4e-2	4.9e-2
MSI($S = 1, \beta = 1, d = 0$)	3.4e-2	5.9e-2
MSI($S = 1, \beta = 1, d = 1$)	1.2e-4	3.0e-4

Table 2: Faculty for attribute control: For CelebA, we use Mutual Information Gap (MIG, Equation (13)) on the ground truth binary labels of CelebA using the auxiliary network. Unlike the various autoencoder architectures, we do not necessarily expect that the semantic attributes learnt will be all-inclusive; so we include the maximum mutual information (third column) over each ground truth attribute and C_i pair to see if any are actually significant. We do see an improvement in disentanglement using architectures with mutual information loss, whereas the discrete-only MSI($S = 1, \beta = 1, d = 1$) discovers semantic attributes that are not aligned with the ground truth attributes. Consequently, for the discrete-only architecture, the MIG measure is inconclusive.

4.4 Qualitative Evaluation

Figures 3 and 4 display example attribute control for the proposed architecture for CelebA. Similar to InfoGAN, we see variables corresponding to emotion and head position; however these correspond to a continuous variable here rather than a categorical variable and exhibit in our case a greater magnitude of control. Surprisingly, the image fourth from the right in Figure 3 appears to also control the glare of the glasses as the head is tilted up. Although some entanglement is still seen, such as the example on the left side of Figure 3, where the faces become more masculine as the orientation

Models	ACM (95% error margin)	Attribute
MSI($S = 0, \beta = 1, d = 0$)	97.0% (3.4%)	Melanin
MSI($S = 1, \beta = 1, d = 0$)	96.0% (3.8%)	Melanin
MSI($S = 1, \beta = 1, d = 1$)	71.0% (8.9%)	Glare

Table 3: Faculty for attribute control: for EyePacs, since attribute labels are not available, we show the results of our Attribute Control Metric (ACM). We see that the discrete-only MSI($S = 1, \beta = 1, d = 1$) performs worse, which, combined with the worse FID scores above, likely indicates that the network was focusing on non-semantically relevant factors to control.

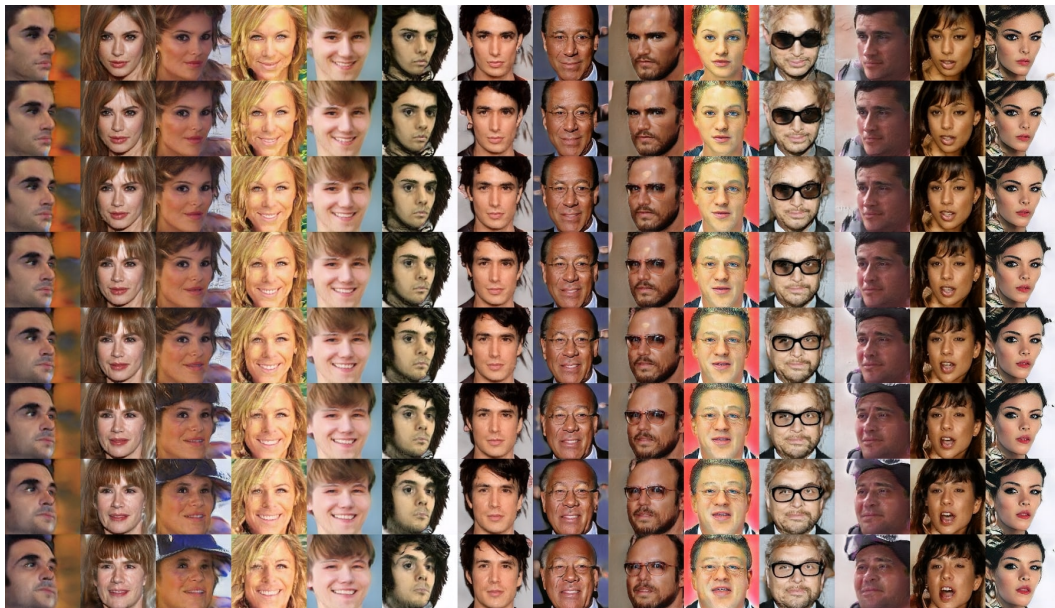


Figure 3: Effects of control and disentanglement by our proposed full featured algorithm MSI($S = 1, \beta = 1, d = 0$) on CelebA showing continuous variable corresponding primarily to control of head orientation (azimuth).

increases, or the fourth from the right on Figure 4 which has glasses appear through increasing the smile. However, across all source images, the effect the attribute control is always very consistent in nature.

In contrast, for the tuned ablated baseline of the algorithm, we see comparatively more entanglement across the various source images. For example, the far left image of Figure 5 has its hair color, gender, and smile all affected, whereas the third from the left has its hair color, head orientation, and smile affected, without affecting the gender. Moreover, as Figures 5 and 6 both use the same latent factors for ablation, we see that the image on the far left in both figures exhibits a similar transformation, despite the control being done on two different variables of c . Consequently, these controls on the tuned baseline do not show a consistent effect like those on the ablated version of the algorithm with style and $\beta = 0$. The continuous variables in both cases exhibited the most interesting factors, whereas the Bernoulli or categorical variables primarily affected the pose.

Moving to EyePACS, most of the Bernoulli variables capture most of the most obvious differences in appearance in these images. For example, Figure 7 controls the color of the retinal image consistently, albeit other factors such as glare are also somewhat affected, and Figure 8 controls the overall brightness of the image. In contrast, continuous variables did not appear to show significant consistent differences beyond having some effect on the blood vessels. The most obvious effect any continuous variable is shown in Figure 9, where some source images, notably the far right and the sixth from the right, have the shape of the retina modified.

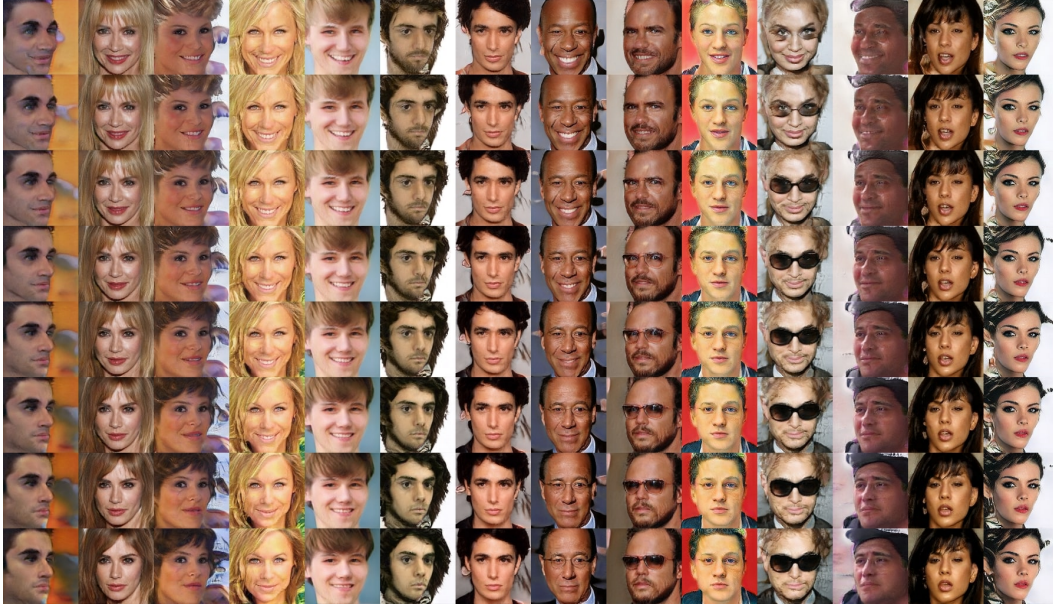


Figure 4: Effects of control and disentanglement by our proposed full featured algorithm $MSI(S = 1, \beta = 1, d = 0)$ on CelebA showing continuous variable control and corresponding effect on smiling and hair color.

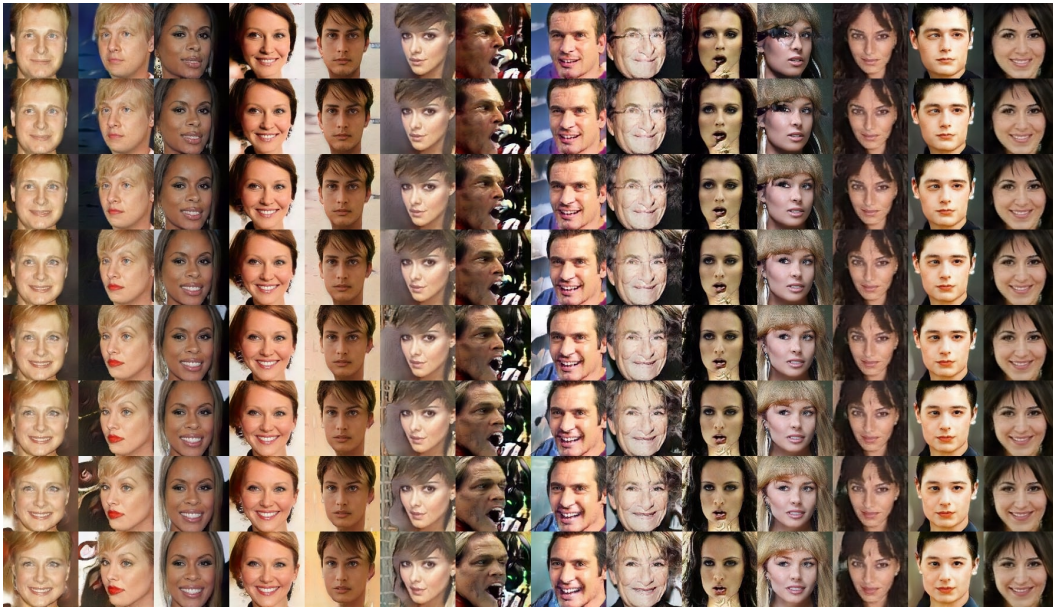


Figure 5: Effects of control and disentanglement by the ablated baseline algorithm $MSI(S = 0, \beta = 1, d = 0)$ on CelebA: Continuous variable controlling gender and smile.

5 Discussion

Visual inspection of our results demonstrates control of semantic variables as well as a good degree of disentanglement for our proposed full fledged model.

This qualitative evidence is also reflected in the competitive quantitative results, more specifically:

CelebA: We found on par FID, i.e., 9.90 for InfoStyleGAN when compared to the ablated baselines (i.e., 9.91 for InfoGAN), while InfoGAN did not perform as well with regard to disentanglement (i.e.,

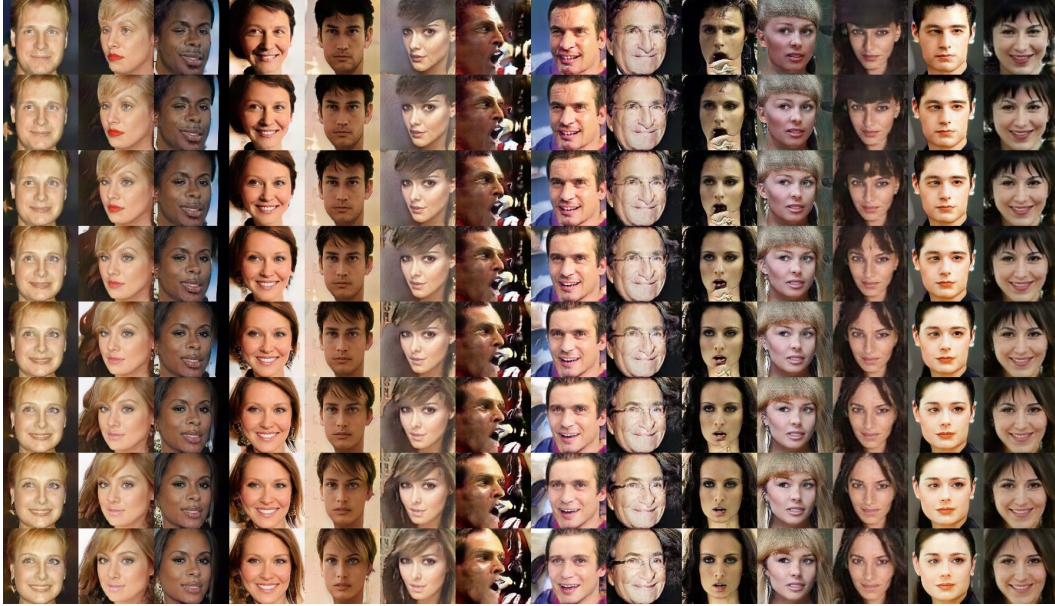


Figure 6: Effects of control and disentanglement by ablated baseline algorithm $MSI(S = 0, \beta = 1, d = 0)$ on CelebA: Continuous variable controlling to hair style.

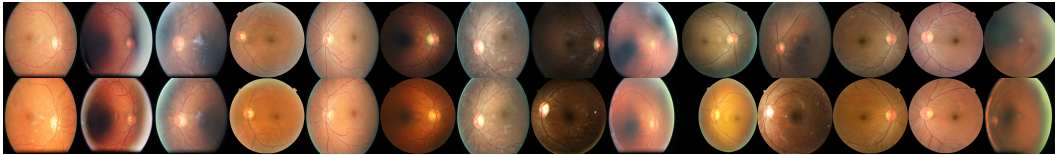


Figure 7: Control by our proposed full featured algorithm $MSI(S = 1, \beta = 1, d = 0)$ for EyePACS using a Bernoulli variable corresponding to ethnicity (Melanin level).

$MIG=3.4e-2$ for InfoStyleGAN, compared to $MIG=2.4e-2$ for InfoStyleGAN). FID was worse for other SOTA algorithms that did not attempt to disentangle, except for COCO-GAN, which uses a much bigger model, so the comparison is not really apple-to-apple.

EyePACS: Results suggest that InfoStyleGAN attribute control (i.e., $ACM=96\%$) is on par with InfoGAN (i.e., $ACM=97\%$) with the difference being within the 95% confidence interval; furthermore, FID for InfoStyleGAN (FID=4.52) is better than for InfoGAN (FID=5.15).

In sum, quantitative and qualitative results suggest the overall benefit of our proposed method.

From Figure 10, we see the information term for the tuned baseline (InfoGAN) actually converges faster, with it being immediately optimized, rather than the gradual increase seen in the InfoStyleGAN architecture. This is likely due to the fact that the latent factors (C) in InfoGAN are fed directly into the generator network once at the beginning, whereas the latent factors in InfoStyleGAN affect the image via linear weightings via the fully connected network. We believe this is a beneficial effect for both control of the semantic attributes and visual quality of the generated images.

Comparing InfoGAN ($MSI(S = 0, \beta = 1, d = 0)$) to our method ($MSI(S = 1, \beta = 1, d = 0)$), we see that InfoGAN does not have the same level of control as InfoStyleGAN likely due to these architectural differences despite comparable visual quality. From the purported benefits of StyleGAN, this disentanglement on the semantic variables is consistent with increased disentanglement of the overall latent space.

Of note, during our experiments we observed that both CelebA and EyePACS did not have L_{info} fully maximized, which explains why some entanglement is still observable in some of the images. This affected EyePACS more, as the continuous variables did not carry as much variation. Consequently an avenue of future work is to address this issue by trying to explicitly minimize total correlation in

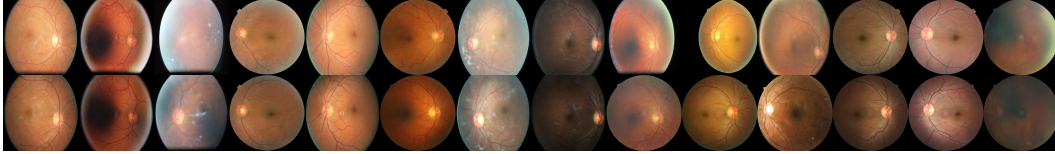


Figure 8: Control by our proposed full featured algorithm $MSI(S = 1, \beta = 1, d = 0)$ for EyePACS using a Bernoulli variable corresponding to brightness.

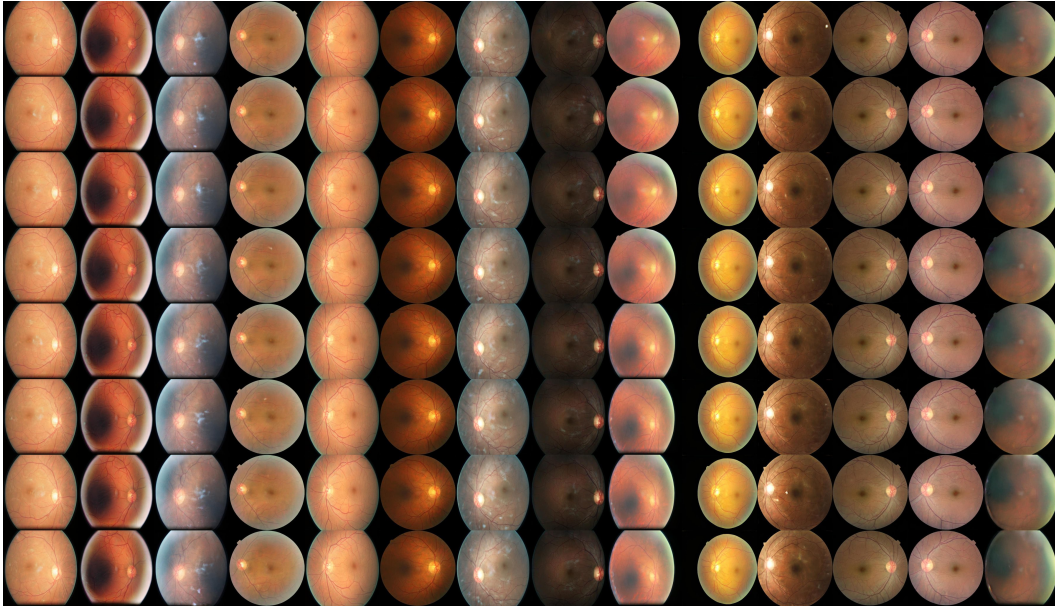


Figure 9: Control by our proposed full featured algorithm $MSI(S = 1, \beta = 1, d = 0)$ for EyePACS using a Continuous variable seemingly controlling shape.

the loss function along with attempting different methods for the maximization of mutual information such as those found in [16].

We also note that CelebA is a more favorable dataset due to greater canonical structure compared to retinal imagery: while eyes have significant levels of variation such as the arrangement of blood vessels, these variations are more subtle compared to faces or imply sharper perceptual transitions. Success of continuous variable versus discrete also points to this. There is also the factor of model mis-specification in the current training in that all variables should be approximated to some degree, rather than some variables being exactly reconstructed and others being ignored.

6 Conclusion

This paper studies focuses on the control of semantic attributes via latent factors. We show that the concepts of control (via mutual information maximization) and disentanglement (via total correlation minimization) are connected as explained in Lemma 3.1. We present an architecture (InfoStyleGAN) exploiting multiscale generative models which maximize mutual information and achieve high resolution image generation along with semantic attribute discovery. Results indicate that the ability of those models to control semantic image attributes entails no significant sacrifice in performance regarding FID, when compared to non-controlling, non-disentangling, state of the art generative methods, with models of similar size (e.g., FID = 9.90 on CelebA and 4.52 on EyePACS.).

References

- [1] A. Brock, J. Donahue, and K. Simonyan. Large scale gan training for high fidelity natural image synthesis. In *ICLR 2019*, June 2019.

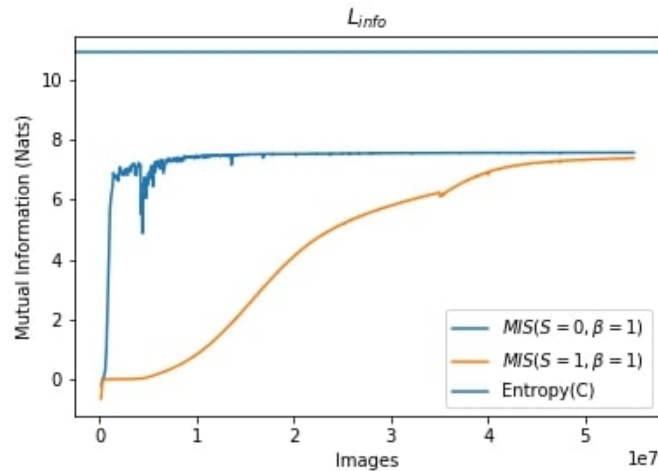


Figure 10: Moving average of L_{info} throughout training. Entropy(C) for discrete C is the upper bound when the mutual information is maximized.

- [2] Tian Qi Chen, Xuechen Li, Roger B Grosse, and David K Duvenaud. Isolating sources of disentanglement in variational autoencoders. In *Advances in Neural Information Processing Systems*, pages 2610–2620, 2018.
- [3] Xi Chen, Yan Duan, Rein Houthoofd, John Schulman, Ilya Sutskever, and Pieter Abbeel. Infogan: Interpretable representation learning by information maximizing generative adversarial nets. In *Advances in neural information processing systems*, pages 2172–2180, 2016.
- [4] J Cuadros and G Bresnick. Eyepacs: An adaptable telemedicine system for diabetic retinopathy screening. *Journal of diabetes science and technology (Online)*, 3(3):509, 2009.
- [5] Ian Goodfellow, Jean Pouget-Abadie, Mehdi Mirza, Bing Xu, David Warde-Farley, Sherjil Ozair, Aaron Courville, and Yoshua Bengio. Generative adversarial nets. In *Advances in neural information processing systems*, pages 2672–2680, 2014.
- [6] Aditya Grover, Manik Dhar, and Stefano Ermon. Flow-gan: Combining maximum likelihood and adversarial learning in generative models. In *Thirty-Second AAAI Conference on Artificial Intelligence*, 2018.
- [7] Tero Karras, Timo Aila, Samuli Laine, and Jaakko Lehtinen. Progressive growing of gans for improved quality, stability, and variation. *arXiv preprint arXiv:1710.10196*, 2017.
- [8] Tero Karras, Samuli Laine, and Timo Aila. A style-based generator architecture for generative adversarial networks. In *Proceedings of the IEEE Conference on Computer Vision and Pattern Recognition*, pages 4401–4410, 2019.
- [9] Tero Karras, Samuli Laine, Miika Aittala, Janne Hellsten, Jaakko Lehtinen, and Timo Aila. Analyzing and improving the image quality of StyleGAN. *CoRR*, abs/1912.04958, 2019.
- [10] Diederik P Kingma and Max Welling. Auto-encoding variational bayes. *arXiv preprint arXiv:1312.6114*, 2013.
- [11] Durk P Kingma and Prafulla Dhariwal. Glow: Generative flow with invertible 1x1 convolutions. In *Advances in Neural Information Processing Systems*, pages 10215–10224, 2018.
- [12] Chieh Hubert Lin, Chia-Che Chang, Yu-Sheng Chen, Da-Cheng Juan, Wei Wei, and Hwann-Tzong Chen. COCO-GAN: generation by parts via conditional coordinating. In *IEEE International Conference on Computer Vision (ICCV)*, 2019.
- [13] Ziwei Liu, Ping Luo, Xiaogang Wang, and Xiaoou Tang. Deep learning face attributes in the wild. In *Proceedings of International Conference on Computer Vision (ICCV)*, December 2015.

- [14] Mario Lucic, Karol Kurach, Marcin Michalski, Sylvain Gelly, and Olivier Bousquet. Are gans created equal? a large-scale study. In *Advances in neural information processing systems*, pages 700–709, 2018.
- [15] Aaron van den Oord, Sander Dieleman, Heiga Zen, Karen Simonyan, Oriol Vinyals, Alex Graves, Nal Kalchbrenner, Andrew Senior, and Koray Kavukcuoglu. Wavenet: A generative model for raw audio. *arXiv preprint arXiv:1609.03499*, 2016.
- [16] B. Poole, S. Ozair, A. van den Oord, A. Alemi, and G. Tucker. On variational bounds of mutual information. In *Proceedings of the 36th International Conference on Machine Learning*, June 2019.
- [17] Tim Salimans, Ian Goodfellow, Wojciech Zaremba, Vicki Cheung, Alec Radford, and Xi Chen. Improved techniques for training gans. In *Advances in neural information processing systems*, pages 2234–2242, 2016.
- [18] H. Zhang, I. Goodfellow, D. Metaxas, and A. Odena. Self-attention generative adversarial networks. In *Proceedings of the 36th International Conference on Machine Learning*, June 2019.